Hindawi
Shock and Vibration
Volume 2024, Article ID 5549976, 21 pages
https://doi.org/10.1155/2024/5549976

Research Article

Research on the Application of Variational Mode Decomposition Optimized by Snake Optimization Algorithm in Rolling Bearing Fault Diagnosis

Houxin Ji, Ke Huang, and Chaoquan Mo

College of Mechanical and Electrical Engineering of Wenzhou University, Wenzhou 325035, China

Correspondence should be addressed to Ke Huang; hk125cn@163.com

Received 19 June 2023; Revised 11 March 2024; Accepted 26 March 2024; Published 5 April 2024

Academic Editor: Giorgio Dalpiaz

The rolling bearing is one of the commonly used mechanical components in rotating machinery, and its health directly affects the normal operation of equipment. However, the fault signal of rolling bearing is susceptible to noise interference, which makes it difficult to extract the fault characteristics of the rolling bearing and thus affects the accuracy of the diagnosis results. To address this problem, this paper proposes a method by using a snake optimization algorithm to optimize variational mode decomposition (SOA-VMD) and applies it to the extraction of the fault feature of rolling bearing. First, the minimum Shannon entropy to kurtosis ratio (EKR) is used as the fitness function of SOA to search for the best parameter combination of VMD. Second, the optimized VMD is used to decompose the vibration signal of rolling bearing to obtain K intrinsic mode functions (IMFs). Then, the IMF with the most fault information is selected for reconstruction through EKR. The Teager–Kaiser energy operator (TKEO) spectrum analysis is performed on the reconstructed signal. Finally, this method is used to analyze the simulation signal and rolling bearing vibration signal and compared with empirical mode decomposition (EMD), ensemble empirical mode decomposition (EEMD), and complete ensemble empirical mode decomposition adaptive noise (CEEMDAN) algorithms to verify the feasibility and effectiveness of the SOA-VMD method.

1. Introduction

Rolling bearings are one of the important components in rotating mechanical equipment and are widely used in various fields such as automobiles, aerospace, and machine tools [1, 2]. Therefore, the health of the rolling bearing determines the operating conditions of most mechanical equipment. Once a rolling bearing fails, the corresponding mechanical equipment will also produce a series of adverse effects. Therefore, it is of great significance to diagnose faults in rolling bearings [3]. The fault signals of rolling bearing usually exhibit nonlinear and nonstationary characteristics and are also easily affected by the environment, resulting in a large amount of noise mixed in the fault signals. This makes it difficult to extract fault features, which in turn affects the diagnosis of rolling bearing faults.

In recent years, many scholars have conducted in-depth research and exploration to address the abovementioned problem and have proposed many methods for extracting fault features of rolling bearings. Hemmati et al. [4] addressed the issue of rolling bearing acoustic emission signals being easily masked by the noise by proposing a method that combines kurtosis with Shannon entropy ratio (EKR) and WPT. This method searches for the best filtering band by combining EKR and WPT, and experiments have shown that this method can effectively extract fault features from noisy acoustic emission signals. Liu et al. [5] proposed an optimized kurtogram method for low-speed rolling bearing acoustic emission signals. First, this method generates an optimized kurtogram with kurtosis to Shannon entropy ratio (KSR) as the optimization goal. Second, it filters out filtering bands with a high signal-to-noise ratio

through KSR. Finally, it uses the envelope spectrum to analyze the acoustic emission signals of the best band. Huang et al. [6] proposed an adaptive decomposition algorithm called empirical mode decomposition (EMD) for nonlinear and nonstationary signals. The main idea of this method is to decompose the signal into a series of intrinsic mode functions (IMFs) that can characterize local features. Based on the above, Tabatabaei Aasi et al. [7] proposed a method combining EMD and EKR. This method first uses EMD to denoise the noisy acoustic emission signals, then selects the best IMF to improve the signal-to-noise ratio through the EKR index, and finally obtains the fault characteristic frequency of the best IMF using envelope spectrum analysis. Experimental results show that the EKR index can effectively select IMF with a high signal-to-noise ratio. However, this method has some drawbacks, such as mode-mixing and end-effects [8]. To address the limitations of EMD, Wu and Huang [9] proposed an ensemble empirical mode decomposition (EEMD) method that adds Gaussian white noise before decomposing the signal to overcome the drawbacks of EMD. Many scholars [10–12] have successfully used this method in fault diagnosis of rolling bearings. While adding white noise can improve the limitations of EMD, it can also significantly affect the decomposition results of fault signals if the white noise coefficient is improperly set [13]. To solve this problem, many scholars [14, 15] have proposed varied solutions.

On this basis, Dragomiretskiy and Zosso [16] proposed a new adaptive decomposition algorithm called variational mode decomposition (VMD) in 2014. This method achieves signal decomposition by constructing and solving variational problems and defining constraints. VMD not only overcomes the limitations of EMD and EEMD but also has advantages such as sound mathematical theory, good signal decomposition performance, and low computational complexity [17]. Mohanty et al. [18] compared VMD and EMD decomposition methods through rolling bearing vibration signals, and the results showed that VMD was superior to EMD in noise robustness and resistance to mode-mixing. Zhang et al. [19] compared VMD and EMD decomposition methods by using a rolling bearing experiment of a multistage centrifugal pump. Zhang et al. [20] combined VMD and majorization-minimization-based total variation and applied it to noisy rolling bearing experiments, and the results showed that this method had good noise robustness. However, VMD also has some shortcomings, the most obvious being that its decomposition performance depends on the choice of parameters such as the number of decomposition levels K and the quadratic penalty factor α. The number of decomposition levels K determines the number of IMF obtained after decomposition [21]. When K is too large, overdecomposition may occur, meaning that the center frequencies of each IMF are close to each other, resulting in mode-mixing. When K is too small, underdecomposition may occur, meaning that some effective information in the original signal may be filtered out. The penalty factor α determines the bandwidth of the center frequency of each IMF [22]. When α is too large, frequency band information may be lost, while when α is too small, redundant information may appear.

To address the parameter selection problem of VMD, Gu et al. [23] proposed a fault feature extraction method based on minimum envelope entropy-optimized VMD. First, this method uses the minimum envelope entropy as the fitness function and uses the gray wolf optimization algorithm to optimize the VMD parameters. Second, it uses the optimized VMD to perform VMD decomposition on the fault signal. Finally, it selects IMF through the weighted kurtosis index (WKI) and extracts fault features using the TKEO envelope spectrum. Zhang et al. [24] proposed a method based on grasshopper optimization algorithm (GOA)-optimized VMD. This method uses the WKI as the optimization goal and optimizes it through the GOA. Finally, it uses WKI to select sensitive IMF and extracts fault features using the Hilbert envelope spectrum. Liu et al. [25] proposed a kurtosis-optimized VMD method for detecting milling chatter. This method sets the step size and then searches for the VMD parameters corresponding to the maximum kurtosis within a certain range. Second, it uses the maximum energy entropy of IMF to filter the results and extract chatter features. Wang et al. [26] proposed a denoising method based on optimized VMD for mining cable partial discharge signals that are easily interfered by noise. This method uses the minimum envelope entropy as the optimization goal and optimizes the VMD parameters through a genetic algorithm. Then, it uses optimized VMD to decompose the signal to obtain multiple IMFs. Afterward, it uses wavelet threshold denoising on each IMF to further eliminate noise. Finally, all denoised IMFs are reconstructed to obtain the final denoised signal. Yang et al. [27] proposed an information entropy-optimized VMD method for bearing vibration signals, combined with kurtosis and correlation coefficient criteria to achieve separation of noise and effective signals. Through simulation and experimental verification, this method can effectively achieve the separation of noise signals. Yi et al. [28] proposed a particle swarm-optimized VMD method, with the optimization goal being the ratio between the mean value and the variance of the cross-correlation coefficient. Li et al. [29] proposed an optimized VMD method with the optimization objective being the maximum envelope entropy. This method sets the step size and range to perform VMD optimization and uses frequency band entropy as the criterion for measuring the effective signal containing the most fault information. Finally, it obtains bearing fault features through envelope spectrum analysis. Shi et al. [30] proposed a method using a niche genetic algorithm (NGA) to optimize VMD. This method uses Shannon entropy as the fitness function and uses NGA to optimize VMD. Then, it extracts energy features from the optimized VMD results and inputs them into an optimized support vector machine for classification. Liang et al. [31] proposed an optimized VMD method by using a multiobjective multi-island genetic algorithm (MIGA). This method uses envelope entropy and Renyi entropy as optimization functions and optimizes VMD through MIGA. This paper uses a novel optimization algorithm called snake optimization algorithm (SOA) to optimize the parameters of VMD. SOA is a new meta-heuristic optimization algorithm proposed by Hashim and Hussien, and inspired by the mating behavior of snakes [32].

This algorithm achieves a good balance between exploration and exploitation, and its superiority and convergence over other optimization algorithms such as TEO, GOA, and WOA have been verified on 30 unconstrained functions and 4 engineering instances.

Based on the abovementioned research, this paper proposes a rolling bearing fault diagnosis method based on the snake optimization algorithm-optimized VMD (SOA-VMD). First, with the minimum EKR value of the intrinsic mode components after VMD decomposition as the optimization objective, the VMD parameters are optimized through the SOA to obtain the optimal parameters α and K. Second, the obtained optimal parameters α and K are substituted into VMD to decompose the fault signal. Then, EKR is used as a screening criterion to filter and reconstruct the modal components obtained by VMD decomposition to reduce possible noise interference. Finally, TKEO energy spectrum analysis is performed on the reconstructed signal to extract the fault characteristic frequency of rolling bearings and achieve fault diagnosis.

The main contributions of this paper are as follows:

(1) A method is proposed that utilizes the EKR index as the optimization objective and uses the snake optimization algorithm to address the VMD parameter selection problem

(2) Through the verification of simulation and experimental signals, the feasibility and effectiveness of this method are demonstrated

(3) The proposed method is compared with other common signal decomposition methods, such as EMD, EEMD, and CEEMDAN, to verify its effectiveness

2. Background Theories

2.1. Basic Principles of the VMD. VMD is an adaptive and nonrecursive signal decomposition algorithm. Its core idea is to construct a constrained variational model and solve it iteratively to decompose a nonlinear and nonstationary signal into multiple IMFs, each of which corresponds to a specific frequency and amplitude. The specific process of this algorithm is as follows [16]:

(1) By analyzing $u_k(t)$ through the Hilbert transform, the unilateral spectrum corresponding to $u_k(t)$ can be obtained as shown in the following equation:

$$\left(\delta(t) + \frac{j}{\pi t}\right) * u_k(t). \tag{1}$$

(2) By adding an exponential term to modulate the center frequency, the spectrum of each IMF is modulated to the baseband, as shown in the following equation:

$$\left[\left(\delta(t) + \frac{j}{\pi t}\right) * u_k(t)\right] e^{-j\omega_k t}. \tag{2}$$

(3) By using the Gaussian smoothness index to demodulate the signal to estimate the bandwidth of each IMF, the constrained variational model is obtained as shown in the following equation:

$$\begin{cases} \min\limits_{\{u_k\},\{\omega_k\}} \left\{ \sum\limits_{k=1}^{K} \left\| \partial_t \left[\left(\delta(t) + \frac{j}{\pi t} \right) * u_k(t) \right] e^{-j\omega_k t} \right\|_2^2 \right\}, \\ \text{s. t.} \quad \sum\limits_{k=1}^{K} u_k(t) = X(t), \end{cases} \tag{3}$$

where K is the number of IMFs, ∂_t is the partial derivative with respect to time, $\delta(t)$ is the impulse function, j is the imaginary number, $u_k(t)$ is the $k-$th IMF, $\omega_k(t)$ is the estimated center frequency of the $k-$th IMF, $X(t)$ is the original signal, and $*$ is the convolution operator.

(4) To obtain the optimal solution, a quadratic penalty factor α and the Lagrange multiplier operator $\lambda(t)$ are introduced to transform the constrained variational problem into an unconstrained optimization problem, as shown in the following equation:

$$\begin{aligned} L(\{u_k\},\{\omega_k\},\lambda) = \alpha \sum_{k=1}^{K} \left\| \partial_t \left[\left(\delta(t) + \frac{j}{\pi t} \right) * u_k(t) \right] e^{-j\omega_k t} \right\|_2^2 \\ + \left\| X(t) - \sum_{k=1}^{K} u_k(t) \right\|_2^2 + \left\langle \lambda(t), X(t) - \sum_{k=1}^{K} u_k(t) \right\rangle, \end{aligned} \tag{4}$$

where α can guarantee the reconstruction accuracy of the signal under Gaussian noise and <·> represents the inner product operator.

(5) The alternating direction method of multipliers (ADMM) is used for iterative updates, and the original signal is decomposed into K-modal components.

2.2. Snake Optimization Algorithm. The SOA is a new metaheuristic algorithm proposed by Hashim and Hussien in 2022. The algorithm simulates the foraging, mating, and reproduction behaviors of snakes and has a fast search rate and high optimization accuracy. The mathematical description of the algorithm is as follows [32]:

(1) Uniformly distributed random snake swarm positions are generated and their corresponding fitness is calculated by using the following formula:

$$\begin{cases} X_i = X_{\min} + \text{rand} * (X_{\max} - X_{\min}), \\ F_i = \text{object}(X_i), \end{cases} \tag{5}$$

where rand is a random number in the range [0, 1], $X_{\min}$ and $X_{\max}$ are the lower and upper bounds of the optimization problem, X_i is the random position of the ith snake, object is the fitness function or objective function, and F_i is the fitness value.

(2) Then, the snake swarm X and fitness values F are divided into two groups of males and females in a 1 : 1 ratio by using the following formula:

$$\begin{cases} X_m = \{X_1, X_2, \cdots, X_{N/2}\}, \\ X_f = \{X_{N/2+1}, \cdots, X_N\}, \\ F_m = \{F_1, F_2, \cdots, F_{N/2}\}, \\ F_f = \{F_{N/2+1}, \cdots, F_N\}, \end{cases} \tag{6}$$

where N is the total number of snakes in the swarm (an integer), X_m and X_f are the male and female groups, and F_m and F_f are the fitness values of the male and female groups.

(3) Now, the best fitness values and food locations are obtained from the male and female groups.

$$\begin{cases} F_{\min} = \text{Min}(F), \\ X_{\text{food}} = \text{pos}(F_{\min}), \\ F_{m\_\min} = \text{Min}(F_m), \\ X_{m\_\text{food}} = \text{pos}(F_{m\_\min}), \\ F_{f\_\min} = \text{Min}(F_f), \\ X_{f\_\text{food}} = \text{pos}(F_{f\_\min}), \end{cases} \tag{7}$$

where $F_{\min}$ is the best fitness of all snake swarms, X_{food} is the location of the best fitness, and $F_{m\_\min}, F_{f\_\min}, X_{m\_\text{food}}$, and X_{f_food} are the best fitness and locations of the male and female groups.

The formula for defining the temperature (Temp) and food quantity (Q) of a snake is as follows:

$$\begin{cases} \text{Temp} = \exp\left(\frac{-t}{T}\right), \\ Q = C_1 * \exp\left(\frac{t-T}{T}\right), \end{cases} \tag{8}$$

where t is the current number of iterations, T is the maximum number of iterations, and the constant is $C_1 = 0.5$.

(4) When $Q < 0.25$ (no food), the snake swarm enters the exploration stage, that is, they choose any position to search for food and update their positions. The position update formula for the male snake swarm is as follows:

$$\begin{cases} X_{m,i} = X_{m,\text{rand}} \pm C_2 A_m [(X_{\max} - X_{\min})\text{rand} + X_{\min}], \\ A_m = \exp\left(\frac{-F_{m,\text{rand}}}{F_{m,i}}\right), \end{cases} \tag{9}$$

where $X_{m,i}$ is the position of the ith male snake in the male swarm, X_{m_rand} is the position of a random male snake, A_m is the ability of the male snake to find food, F_{m_rand} is the fitness of $X_{m\_\text{rand}}, F_{m,i}$ is the fitness of the ith male snake, and the constant is $C_2 = 0.05$.

Similarly, the position update formula for the female group is as follows:

$$\begin{cases} X_{f,i} = X_{f,\text{rand}} \pm C_2 A_f [(X_{\max} - X_{\min})\text{rand} + X_{\min}], \\ A_f = \exp\left(\frac{-F_{f,\text{rand}}}{F_{f,i}}\right). \end{cases} \tag{10}$$

When $Q > 0.25$ (food exists) and Temp > 0.6 (hot state), the snake swarm enters the development phase; that is, the snake swarm only moves in the direction of food, as shown in the following formula:

$$X_{i,j}(t+1) = X_{\text{food}} \pm C_3 * \text{Temp} * \text{rand} * \left(X_{\text{food}} - X_{i,j}(t)\right), \tag{11}$$

where $X_{i,j}$ is the jth position of the ith snake in the snake swarm and the constant is $C_3 = 2$.

When $Q > 0.25$ and Temp < 0.6 (cold state), the snake group is in a fighting and mating mode. For the male snake group, the fighting mode formula is as follows:

$$\begin{cases} X_{m,i}(t+1) = X_{m,i}(t) + C_3 L_m * \text{rand} * \left(Q * X_{f\_\text{food}} - X_{m,i}(t)\right), \\ L_m = \exp\left(\dfrac{-F_{f\_\min}}{F_i}\right), \end{cases} \tag{12}$$

where L_m is the fighting ability of the male snake.

Similarly, the formula for the combat mode of the female snake group is as follows:

$$\begin{cases} X_{f,i}(t+1) = X_{f,i}(t) + C_3 L_f * \text{rand} * \left(Q * X_{m\_\text{food}} - X_{f,i}(t)\right), \\ L_f = \exp\left(\dfrac{-F_{m\_\min}}{F_i}\right). \end{cases} \tag{13}$$

The mating mode formula for the male snake swarm is as follows:

$$\begin{cases} X_{m,i}(t+1) = X_{m,i}(t) + C_3 M_m \text{rand} * \left(Q X_{f,i}(t) - X_{m,i}(t)\right), \\ M_m = \exp\left(\dfrac{-F_{f,i}}{F_{m,i}}\right), \end{cases} \tag{14}$$

where M_m is the mating ability of the male snake.

Similarly, the pairing mode formula for the female snake group is as follows:

$$\begin{cases} X_{f,i}(t+1) = X_{f,i}(t) + C_3 M_f \text{rand} * \left(Q X_{m,i}(t) - X_{f,i}(t)\right), \\ M_f = \exp\left(\dfrac{-F_{m,i}}{F_{f,i}}\right). \end{cases} \tag{15}$$

After the mating mode, if the snake eggs hatch successfully, a snake with the worst fitness will be selected from both the male and female snake swarms for replacement. The replacement formula is as follows:

$$\begin{cases} X_{m\_\text{worst}} = X_{\min} + \text{rand} * (X_{\max} - X_{\min}), \\ X_{f\_\text{worst}} = X_{\min} + \text{rand} * (X_{\max} - X_{\min}), \end{cases} \tag{16}$$

where X_{m_worst} and X_{f_worst} are the snakes with the worst fitness in the male and female groups.

2.3. Teager–Kaiser Energy Operator. TKEO is a nonlinear differential operator proposed by Kaiser in 1990 for calculating signal energy. It can reflect the impact characteristics of signals and has the advantages of simple operation and high time resolution [33]. In recent years, this algorithm has been widely used in the field of rolling bearing fault diagnosis.

For continuous signals $g(t)$, the TKEO calculation formula is as follows:

$$T[g(t)] = [g'(t)]^2 - g(t) * g''(t), \tag{17}$$

where $g'(t) = \mathrm{d}g/\mathrm{d}t$, $g''(t) = d'g/\mathrm{d}t$.

For discrete signals $X(n)$, the TKEO calculation formula is as follows:

$$T[X(n)] = [X(n)]^2 - X(n+1) * X(n-1). \tag{18}$$

2.4. Shannon Entropy to Kurtosis Ratio (EKR)

2.4.1. Shannon Entropy. Shannon entropy was first proposed in communication theory to describe the complexity of observed signal sequences. The smaller the entropy value, the more ordered the signal, and the larger the entropy value, the more complex the signal [34, 35]. In statistics, Shannon entropy is also considered as a measure of information loss of random variables. In the case of rolling bearing, when a defect occurs, the defect surface collides periodically with other components, producing evenly spaced pulses. Therefore, the smaller the Shannon entropy value of the rolling bearing signal, the higher the concentration of signal energy and signal-to-noise ratio, and the more effective information it contains.

Let the discrete signal be $X(t) = \{x_1, x_2, \ldots, x_N\}$, and the mathematical description of Shannon entropy is as follows:

$$\begin{cases} E = -\sum_{i=1}^{N} p_i * \log_2 p_i, \\ p_i = \dfrac{(x_i)^2}{\sum_{i=1}^{N} (x_i)^2}, \\ \text{s.t.} \sum_{i=1}^{N} p_i = 1, \end{cases} \tag{19}$$

where p_i is the probability distribution of $X(t)$.

2.4.2. Kurtosis. Kurtosis is a dimensionless index used to characterize the flatness of a waveform, and its mathematical expression is shown as follows:

$$K = \frac{1}{N} \sum_{i=1}^{N} \left(\frac{x_i - \bar{X}}{\sigma} \right)^4, \tag{20}$$

where $\overline{X}$ is the mean value of the signal and σ is the standard deviation of the signal.

In the diagnosis of the rolling bearing fault, kurtosis, as a dimensionless index, is not only unaffected by parameters such as bearing speed, size, and load but also very sensitive to impact signals, making it particularly suitable for judging rolling bearing damage [36, 37]. When the rolling bearing operates normally, due to the influence of some uncertain factors, its signal amplitude follows a normal distribution, so the kurtosis value is approximately 3. However, when the rolling bearing is damaged, the damage will cause the signal amplitude to increase, causing the amplitude to deviate from the normal distribution, thereby increasing the kurtosis value. The larger the kurtosis value, the more severe the rolling bearing fault and the more fault information the signal contains.

2.4.3. EKR. Shannon entropy and kurtosis are both indicators used to reflect the sequentiality and distribution of signals. Therefore, combining them can provide a more comprehensive signal evaluation. Considering the sequentiality and distribution of signals comprehensively can help us to understand the characteristics of signals more fully, thus enabling more accurate signal analysis and processing. Its mathematical expression is as follows:

$$\begin{aligned} \text{EKR} &= \frac{\text{Shannon entropy}}{\text{kurtosis}} \\ &= \frac{E}{K}. \end{aligned} \tag{21}$$

3. Procedure of the Proposed Method

The two key parameters of VMD, namely, the decomposition level K and the quadratic penalty factor α, have a significant impact on the signal decomposition results. In order to obtain suitable parameters, this paper uses the minimum EKR value as the fitness function of the optimization algorithm and uses SOA to optimize the K and α of VMD. EKR combines the advantages of Shannon entropy and kurtosis indexes, so it can provide a more comprehensive signal evaluation. When the EKR value of the signal is smaller (Shannon entropy is smaller and kurtosis is larger), the signal contains more effective information and is more helpful for subsequent analysis. The specific optimization steps are as follows:

(1) The snake swarm of SOA is initialized and the parameters of VMD are optimized. The specific parameters are shown in Table 1. In Table 1, Dim represents the dimension, X represents the number

of snake swarms, T represents the maximum number of iterations, t represents the current number of iterations, and $X_{\min}$ and $X_{\max}$ represent the optimization range of α and K.

(2) The snake swarm is divided according to equation (6) and the fitness function is calculated to obtain the EKR value.

(3) We then find the best fitness value and its position according to equation (7).

(4) The temperature (Temp) and food quantity (Q) are then calculated according to equation (8).

(5) The corresponding stage is entered according to the conditions satisfied by Q, Temp, and Rand to perform the corresponding actions.

(6) Steps 3–5 are then repeated until the maximum number of iterations is reached.

(7) Finally, the position of the snake swarm is given as output, that is, the parameters K and α after VMD optimization.

The flowchart of the method proposed in this paper is shown in Figure 1. The detailed steps are as follows:

(1) Vibration signals from rolling bearings are collected.

(2) The basic parameters of SOA are then set according to Table 1.

(3) SOA is used to optimize the VMD parameters to obtain the optimized K and α;

(4) Optimized VMD is used to decompose the vibration signal to obtain K IMFs.

(5) The EKR index of each IMF is then calculated and the IMF corresponding to the minimum EKR value is selected as the effective component.

(6) TKEO is used to calculate the energy of the effective component.

(7) FFT transform is then performed on the result of step 6 to obtain the TKEO spectrum.

(8) Lastly, the characteristic frequency of the TKEO energy spectrum is extracted and compared with the theoretical fault characteristic frequency to determine the fault type of rolling bearing.

4. Simulation Analysis

To verify the effectiveness of the method proposed in this paper, the rolling bearing inner ring fault simulation model proposed by Randall et al. [38] was used for verification. The model takes into account the influence of factors such as rolling bearing structure, manufacturing tolerances, random sliding of balls, and surface wear. The mathematical expression of the inner ring fault simulation model is as follows:

Table 1: Parameter initialization of the snake optimizer.

Parameters	Values
Dim	2
X	30
T	50
t	0
$X_{\min}$	[100, 2]
$X_{\max}$	[3000, 13]

$$\begin{cases} A_i(t) = A_0 \cdot \cos\left(2\pi f_r + \varphi_A\right) + C_A, \\ p(t) = \exp\left(-\mathrm{Bt}\right) \cdot \cos\left(2\pi f_n t + \varphi_w\right), \\ x(t) = \sum A_i(t) \cdot p(t - iT) + n(t), \end{cases} \tag{22}$$

where $A_i(t)$ is the amplitude modulation function, f_r is the rotation frequency, C_A is an arbitrary coefficient, $p(t)$ is the impact signal caused by defects, t is the time period of the impact signal, f_n is the resonance frequency, T is the average period of the pulse sequence, and $n(t)$ is Gaussian white noise.

In order to simulate the noise impact in actual acquisition, −12 dB Gaussian noise was added to the simulation signal. The specific parameters are shown in Table 2.

Figure 2 shows the time-domain waveform and envelope spectrum of the simulation signal. As shown in Figure 2(c), the periodic impact signal in the time-domain waveform is masked by noise. As shown in the envelope spectrum in Figure 2(d), although the fault characteristic frequency of the simulation signal can be observed, there are many interference frequencies with higher amplitudes around it, which affects the accuracy of fault identification.

The proposed method is applied to analyze the simulation signal. The SOA parameters are initialized as shown in Table 1, and the convergence curve of the optimized SOA is shown in Figure 3. The minimum EKR found by SOA corresponds to the optimal VMD parameters [K, α] of 2.8329 and [7, 597], respectively. The simulation signal is decomposed by using the optimal VMD parameters, and the decomposition results are shown in Figure 4. According to the description in Section 3, the minimum EKR value is used as a measure of the measurement index containing the most fault information, and the EKR calculation results are shown in Table 3. The IMF4 with the smallest EKR value is selected for the envelope spectrum analysis. Figure 5 shows the time-domain waveform and envelope spectrum of IMF4. As shown in Figure 5(b), in the envelope spectrum of IMF4, the rotation frequency of 35 Hz and the fault characteristic frequency and its harmonics (180 Hz, 360 Hz, and 540 Hz) can be accurately extracted.

To verify the effectiveness of the proposed method, the proposed method is compared with EMD, EEMD, and CEEMDAN methods. First, the EMD method is used for analysis. Figure 6 shows the first 3 IMF results after the simulation signal is decomposed by EMD. As shown in

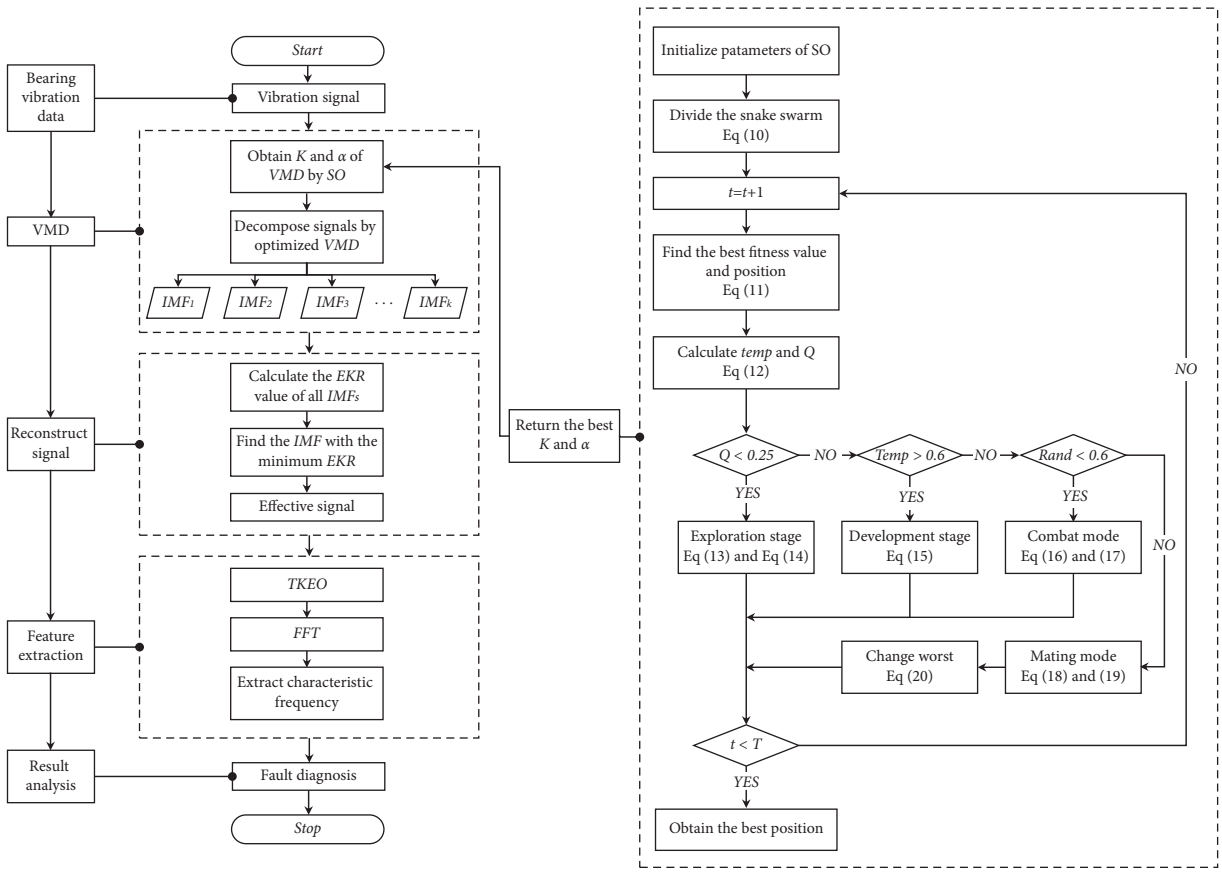

Figure 1: Flowchart of the proposed method.

Table 2: Parameters of the inner ring fault model.

Parameters	Values
Amplitude A_0	1.5
Rotational frequency f_r (Hz)	35
C_A	1
Damping coefficient B	800
Resonance frequency f_n (Khz)	4
Fault characteristic frequency f_i (Hz)	180

Figure 6, the rotational frequency *fr* and fault characteristic frequency *fi* can be extracted from the envelope spectrum of IMF1. However, due to the influence of noise, it is difficult to observe the amplitude of *fr* and *fi* in the envelope spectrum of IMF2 and IMF3. Second, the EEMD method is used and a white noise of 0.15 and an ensemble size of 150 are added [39]. Figure 7 shows the first 4 IMF results after the simulation signal is decomposed by EEMD. As shown in Figure 7, due to the influence of noise, only the rotational frequency *fr*, fault characteristic frequency *fi*, and weak 2*fi* can be extracted from the envelope spectrum of IMF1 and IMF2. Finally, the CEEMDAN method is used for analysis, with added white noise of 0.15 and ensemble size and screening iteration values set to 500 and 5000 [40]. Figure 8 shows the first 4 IMF results after the simulation signal is decomposed by CEEMDAN. As shown in Figure 8, rotational frequency *fr*, fault characteristic frequency *fi*, and 2*fi* can be extracted from the envelope spectrum of IMF1. However, there are still many noise frequencies in the envelope spectrum.

Thus, the proposed method can effectively extract the fault characteristic frequency of the simulation signal under noise interference, and compared to the other three methods, it has more obvious advantages.

5. Experiment Analysis

In this section, the proposed method is applied to the fault signals of the outer and inner rings of rolling bearings, and compared with three other fault feature extraction methods to verify the feasibility of the method. The rolling bearing dataset comes from the fault data collected by the Precision Metrology Laboratory, Mechanical Engineering Department of Sant Longowal Institute of Engineering and Technology in India [41, 42]. The test rig is shown in Figure 9. The experiment prefabricated fault defects on the outer and inner rings of rolling bearings using electrical discharge machining technology. The defect widths were 0.86 mm and 1.01 mm, respectively, and the defect diagrams are shown in Figure 10. The vibration signal of the test bearing is collected by an accelerometer with a sampling frequency of 70 KHz. The radial load of the bearing is 200 N and the speed is

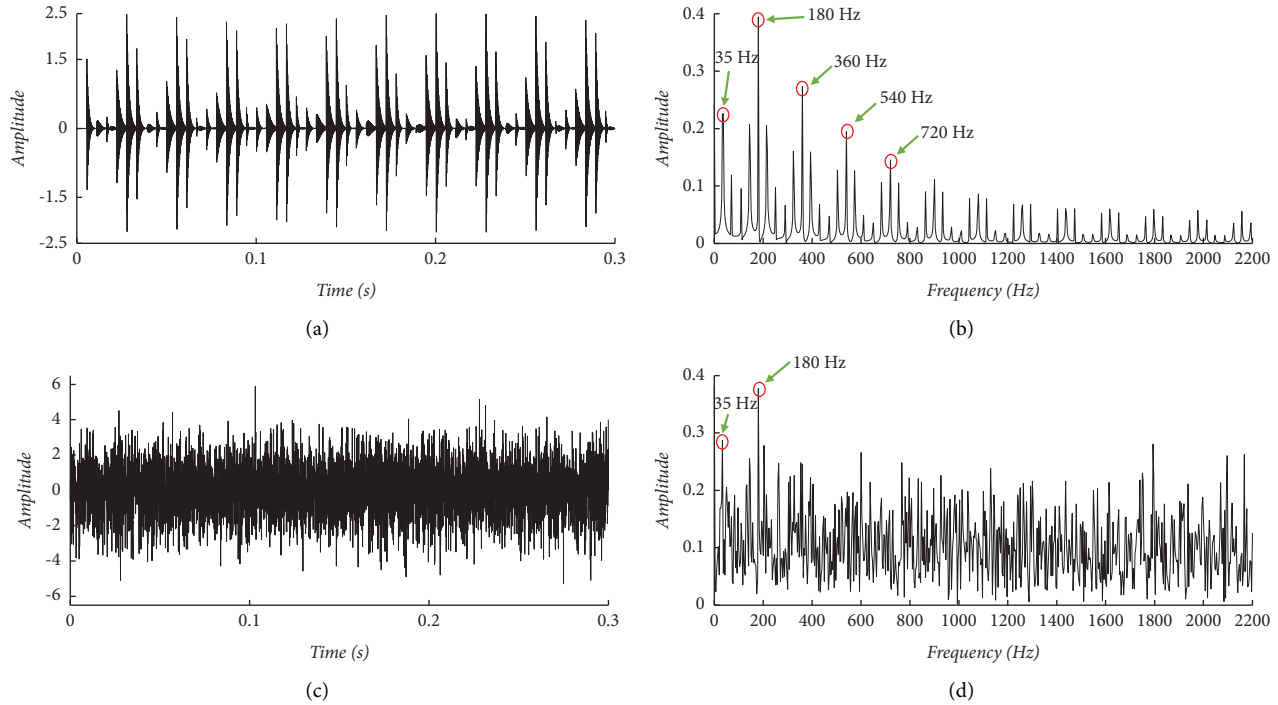

Figure 2: Time-domain waveform and TKEO envelope spectrum of the simulation signal. (a) Time-domain waveform of the origin signal. (b) TKEO envelope spectrum of the origin signal. (c) Time-domain waveform of the signal with added noise. (d) TKEO envelope spectrum of the noise signal.

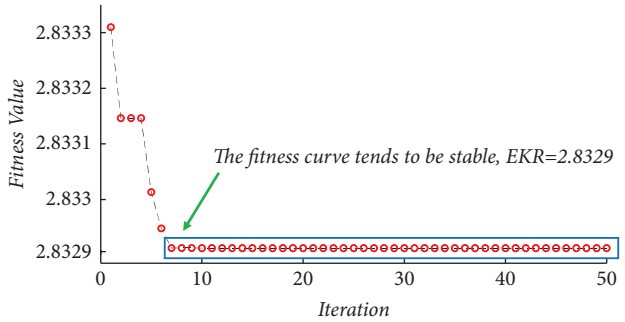

Figure 3: Fitness convergence curve.

2050 r/min. The bearing type is NBC-NU205E, and the specifications are shown in Table 4. The theoretical fault characteristic frequency of the bearing is calculated by using the following equation, and the outer ring fault characteristic frequency is $f_o = 179.3$ Hz, and the inner ring fault characteristic frequency is $f_i = 264.9$ Hz.

$$\begin{cases} f_r = \dfrac{N}{60}, \\ f_o = \dfrac{f_r \cdot Z}{2}\left(1 + \dfrac{d}{D} \cdot \cos\alpha\right), \\ f_i = \dfrac{f_r \cdot Z}{2}\left(1 - \dfrac{d}{D} \cdot \cos\alpha\right), E \end{cases} \tag{23}$$

where f_r is the shaft rotational frequency, N is the rotational speed of the shaft, fo is the outer ring fault characteristic frequency, Z is the number of rolling elements, d is the rolling element diameter, D is the bearing pitch diameter, α is the contact angle, and fi is the inner ring fault characteristic frequency.

5.1. Fault Analysis of the Outer Ring of the Bearing. Figure 11 shows the time-domain waveform and envelope spectrum of the original bearing outer ring fault vibration signal. From Figure 11(c), it can be observed that after adding Gaussian white noise, the features of the high-amplitude and periodic impact signal are masked by the noise. From the envelope spectrum in Figure 11(d), it can be observed that the outer ring fault frequency is not very

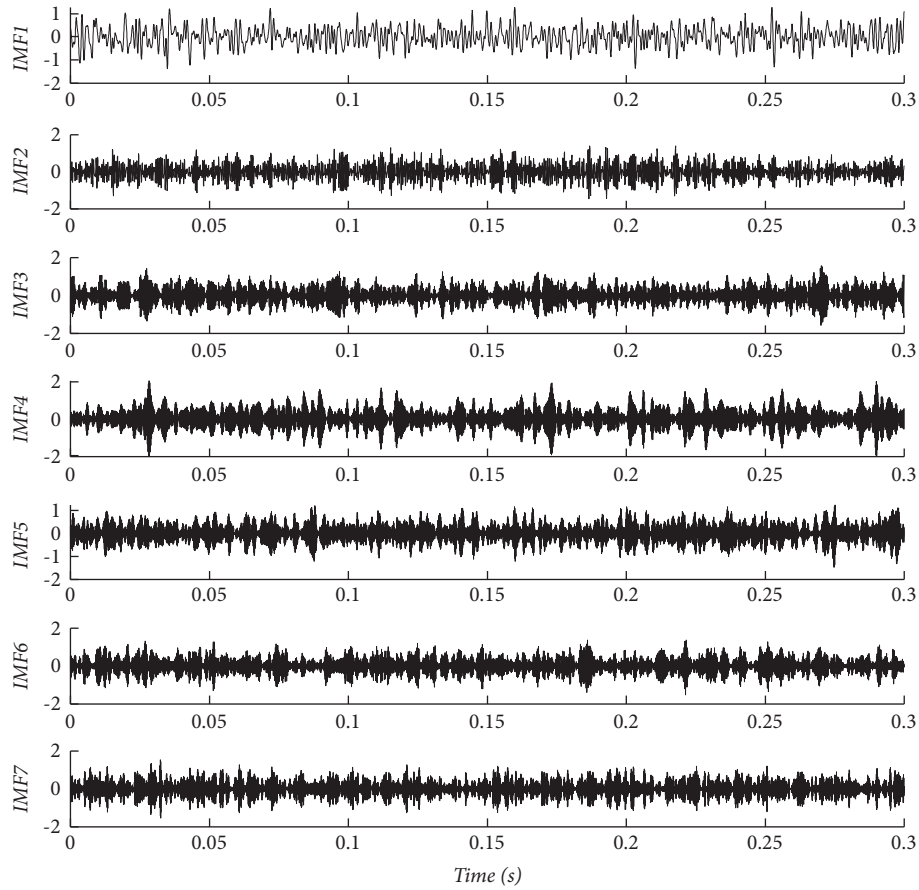

Figure 4: The result of decomposing the noise signal by VMD.

Table 3: The EKR value of each IMF.

IMF	EKR
IMF1	3.6633
IMF2	3.6773
IMF3	3.8197
IMF4	2.8329
IMF5	3.8534
IMF6	3.6750

obvious, and there is noise interference around the fault characteristic frequency.

The proposed method is applied to the analysis of the abovementioned outer ring fault signal. The SOA parameters are set in accordance with Section 4. After SOA optimization, the convergence curve is shown in Figure 12, and the minimum EKR value obtained is 2.7544, corresponding to the optimal VMD parameters $[K, \alpha]$ of [10, 126]. The noisy outer ring fault signal is decomposed by using the optimal VMD parameters, and the decomposition results are shown in Figure 13. The EKR values of all IMFs are calculated, and the results are shown in Table 5. The IMF5 with the smallest EKR value is selected for the envelope spectrum analysis. Figure 14 shows the time-domain waveform and envelope spectrum of IMF5. As shown in Figure 14(b), the fault feature frequency *fo* related to the outer ring fault and its harmonic components can be clearly observed.

To further verify the feasibility of the proposed method, it is compared with the EMD, EEMD, and CEEMDAN methods, where the decomposition parameters of EEMD and CEEMDAN are the same as those in Section 4. Figure 15 shows the first 4 IMF results after the outer ring fault signal is decomposed by EMD. As can be seen from Figure 15, under the influence of noise, only the outer ring fault frequency *fo* and its second harmonic 2*fo* can be extracted from the envelope spectrum of IMF1. Figure 16 shows the first 4 IMF results after the outer ring fault signal is decomposed by EEMD. As shown in Figure 16, the outer ring fault frequency *fo* and its third harmonic 3*fo* can be extracted from the envelope spectrum of IMF1. Figure 17 shows the results after CEEMDAN decomposition. As shown in Figure 17, only the outer ring fault frequency *fo* and its second harmonic 2*fo* can be extracted from IMF1.

Thus, the analysis of the outer ring fault signal further verifies the effectiveness of the proposed method. At the same time, the comparison with the other three methods further highlights the advantages of this method.

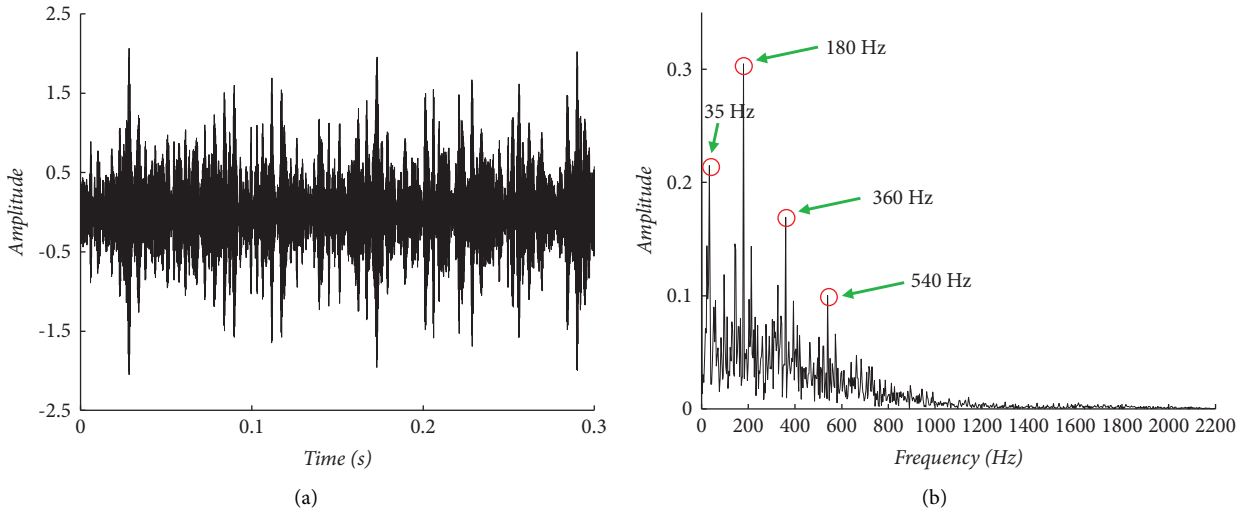

Figure 5: IMF4 reconstructed signal. (a) Time-domain waveform. (b) TKEO envelope spectrum.

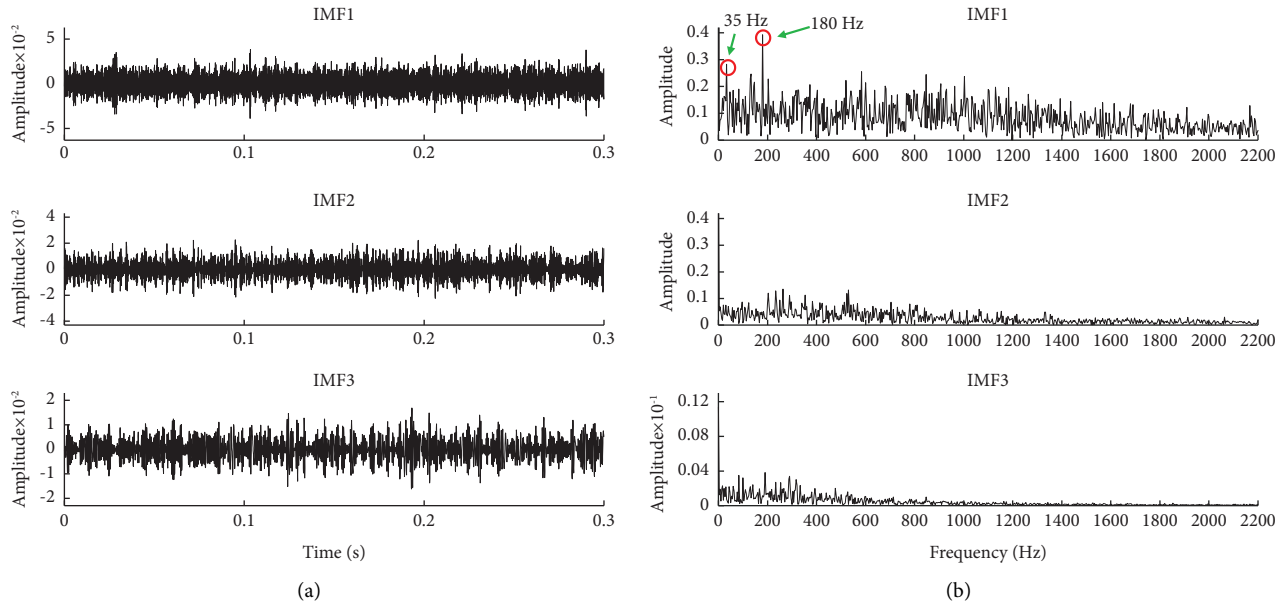

Figure 6: The result of decomposing the noise signal by EMD. (a) Time-domain waveform. (b) TKEO envelope spectrum.

5.2. Fault Analysis of the Inner Ring of the Bearing. Figure 18 shows the time-domain waveform and envelope spectrum of the bearing inner ring fault vibration signal. In Figure 18(c), we can observe that after adding noise, the original periodic impact signal is weakened. As shown in the envelope spectrum in Figure 18(d), the rotational frequency fr and its second harmonic $2fr$ can be extracted.

The proposed method is used to analyze the inner ring fault signal. The SOA parameters are set in accordance with Section 4. The convergence curve after SOA optimization is shown in Figure 19, with the minimum EKR value being 1.9434 and the corresponding optimal parameter set $[K, \alpha]$ being [12, 421]. The VMD method with the optimal parameter set is used to decompose the noisy inner ring fault signal, and the decomposition results are shown in Figure 20. The EKR values of all IMFs are calculated, and the results are shown in Table 6. The IMF5 with the smallest EKR value is selected for envelope spectrum analysis. Figure 21 shows the time-domain waveform and envelope spectrum of IMF5. As shown in Figure 21(b), the rotational frequency fr and three harmonic components related to the inner ring fault characteristic frequency can be clearly identified.

As shown in Section 5.1, the proposed method is compared with three other methods. Figure 22 shows the results after the inner ring fault signal is decomposed by EMD. As shown in Figure 22, only the rotational frequency fr and the inner ring fault characteristic frequency fi can be observed from the envelope spectrum of IMF1. Figure 23 shows the results after the inner ring fault signal is decomposed by EEMD. As shown in Figure 23, the

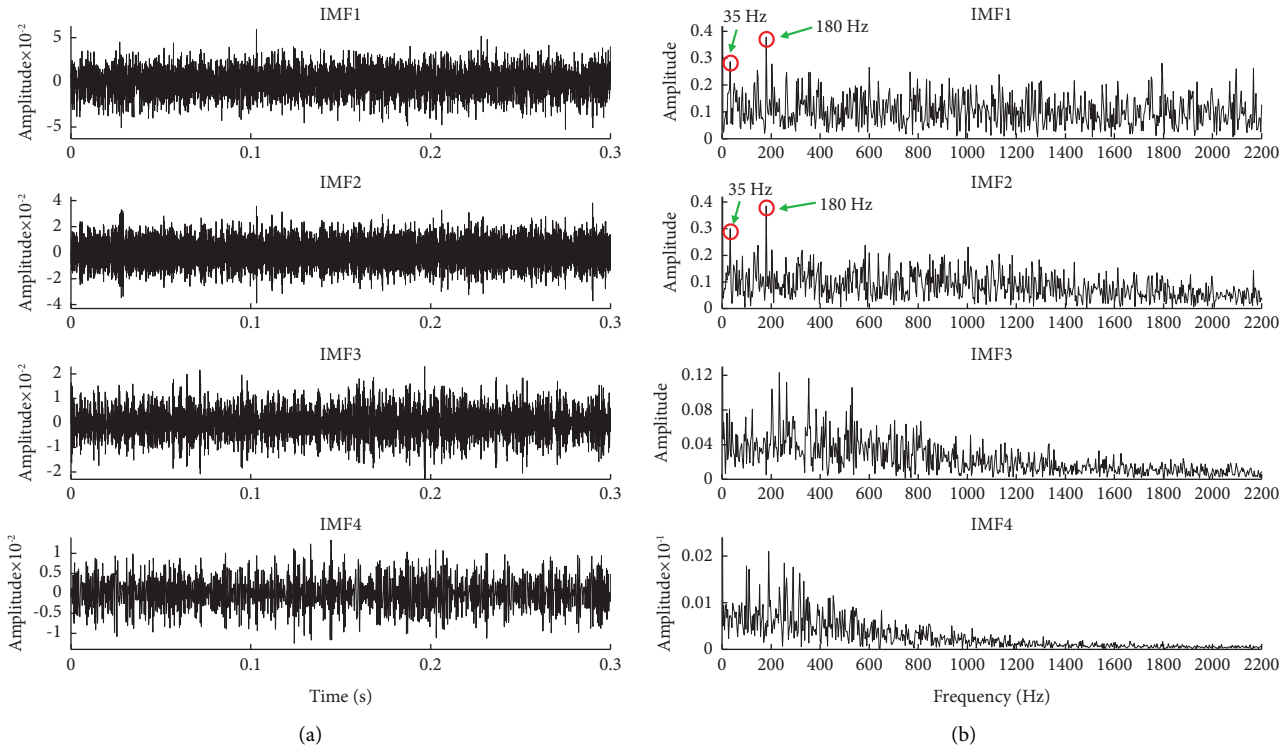

Figure 7: The result of decomposing the noise signal by EEMD. (a) Time-domain waveform. (b) TKEO envelope spectrum.

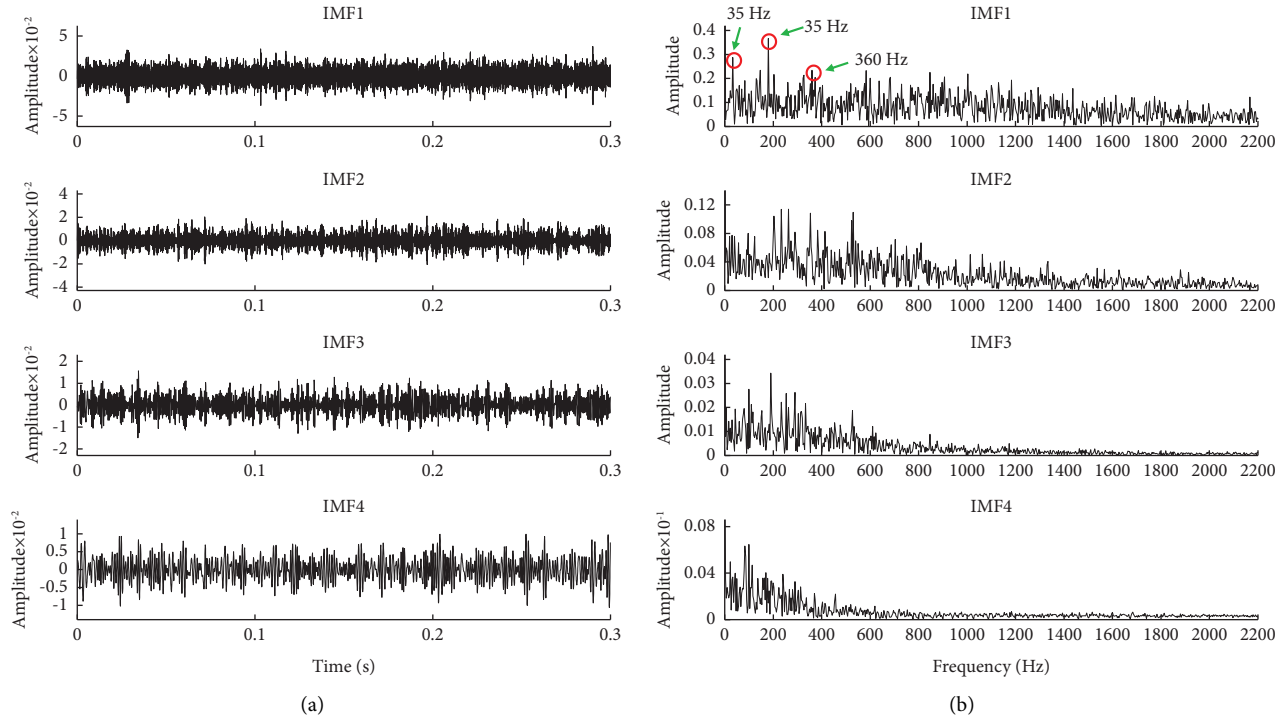

Figure 8: The result of decomposing the noise signal by CEEMDAN. (a) Time-domain waveform. (b) TKEO envelope spectrum.

rotational frequency *fr*, inner ring fault characteristic frequency *fi*, and its second harmonic 2*fi* can be extracted from the envelope spectrum of IMF1 and IMF2. However, it is worth noting that there are other amplitude interferences near *fi* and 2*fi*, which may affect the accuracy of identification. Figure 24 shows the decomposition results of

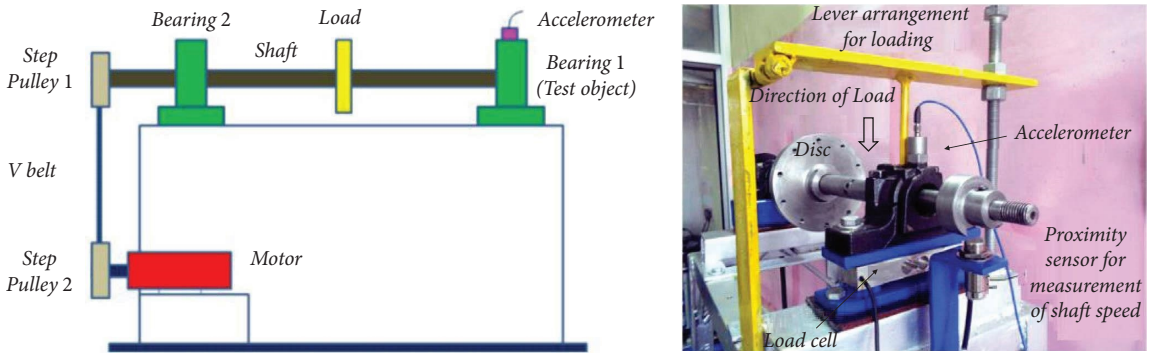

Figure 9: Rolling element bearing test rig. (a) Structural diagram of the test rig. (b) Test rig.

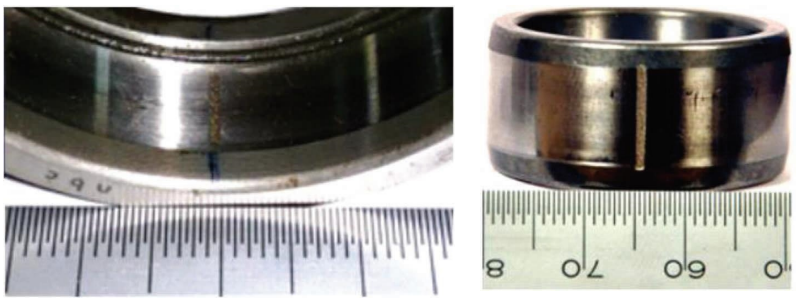

Figure 10: Rolling element bearing test rig. (a) Outer ring defect. (b) Inner ring defect.

Table 4: Structural parameters of NU205E bearing.

Parameters	Values
Outer diameter (mm)	52
Inner diameter (mm)	25
Pitch diameter D (mm)	38.9
Diameter of cylindrical roller d (mm)	7.5
Number of cylindrical roller Z	13
Contact angle α (°)	0

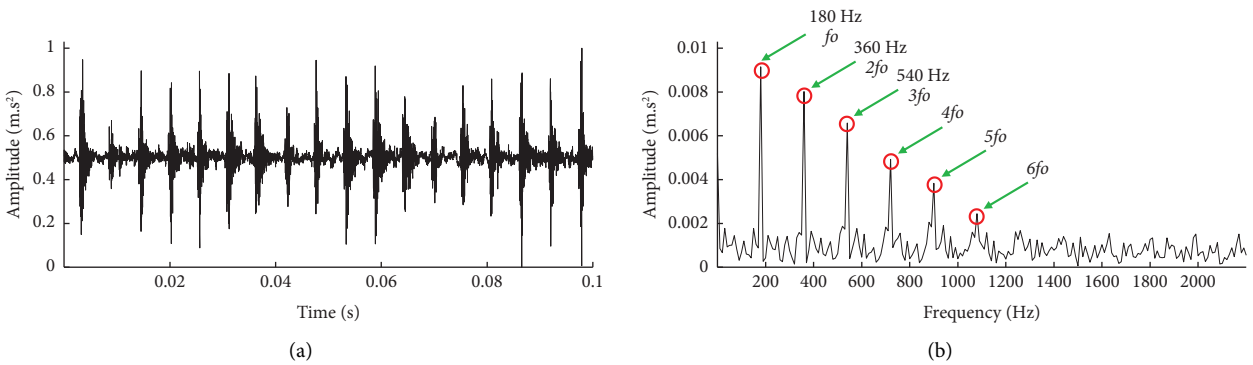

Figure 11: Continued.

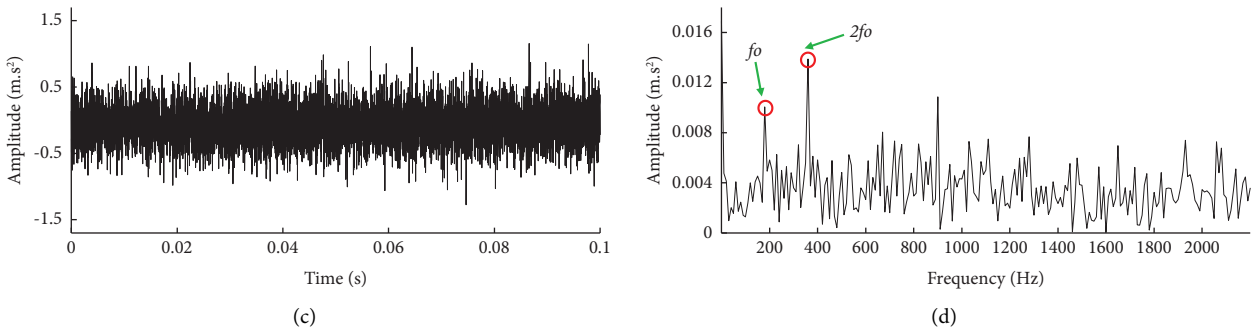

Figure 11: Time-domain waveform and TKEO envelope spectrum of the outer ring defect. (a) Time-domain waveform of the origin signal. (b) TKEO envelope spectrum of the origin signal. (c) Time-domain waveform of the signal with added noise. (d) TKEO envelope spectrum of the noise signal.

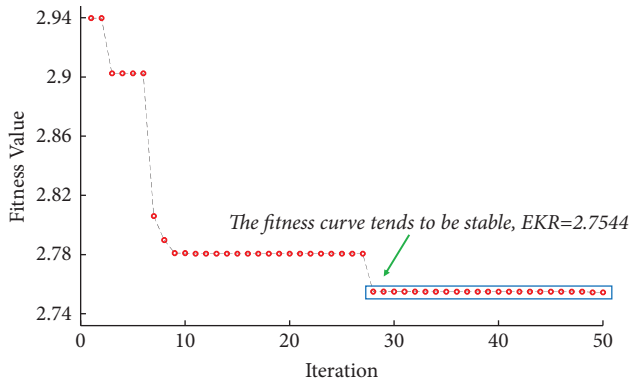

Figure 12: Fitness convergence curve.

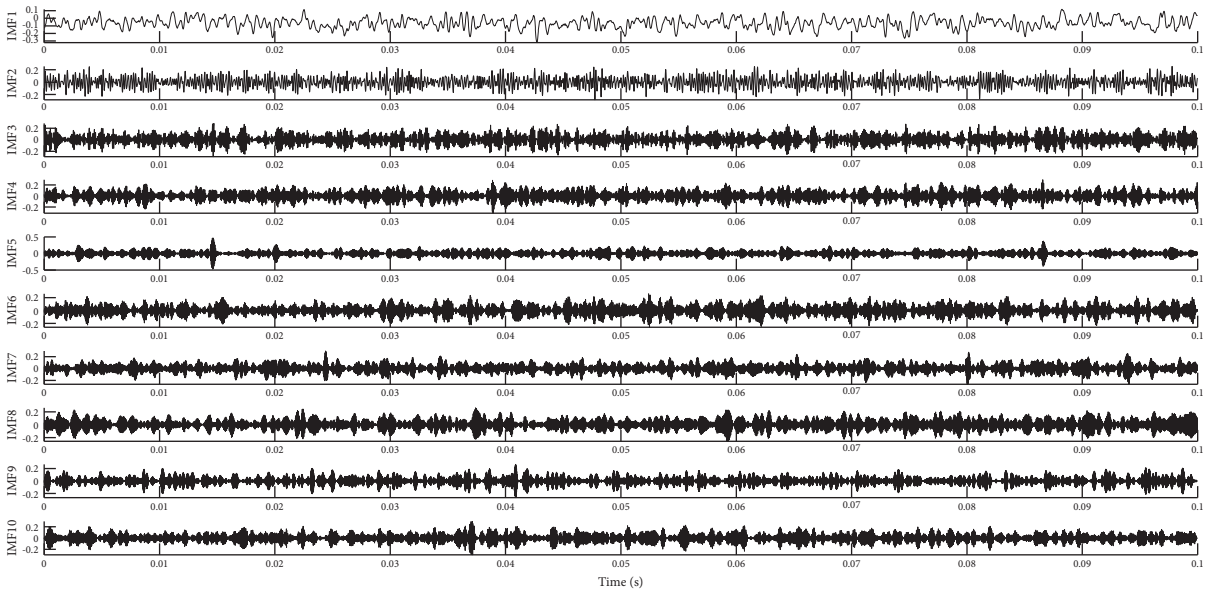

Figure 13: The result of decomposing the outer ring noise signal by VMD.

Table 5: The EKR value of each IMF.

IMF	EKR
IMF1	3.9547
IMF2	4.0052
IMF3	4.0448
IMF4	3.9987
IMF5	2.7544
IMF6	3.9271
IMF7	3.6833
IMF8	3.8795
IMF9	3.8075
IMF10	3.6933

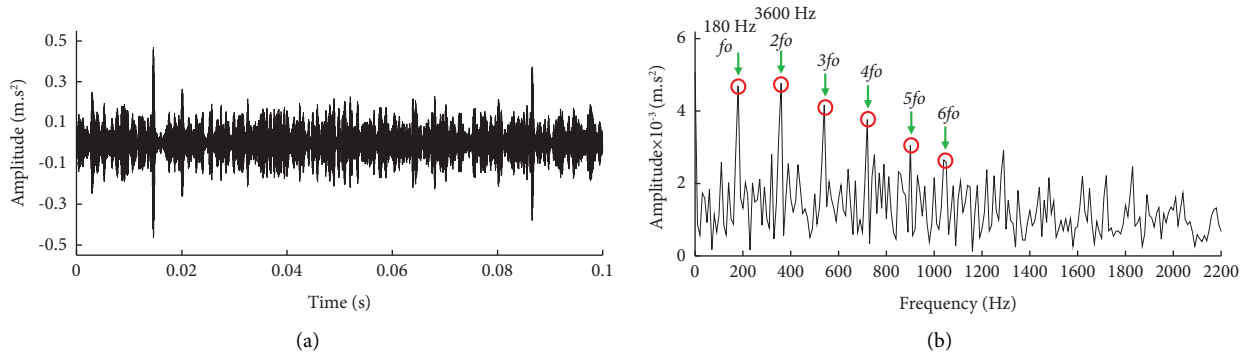

Figure 14: IMF5 reconstructed signal. (a) Time-domain waveform. (b) TKEO envelope spectrum.

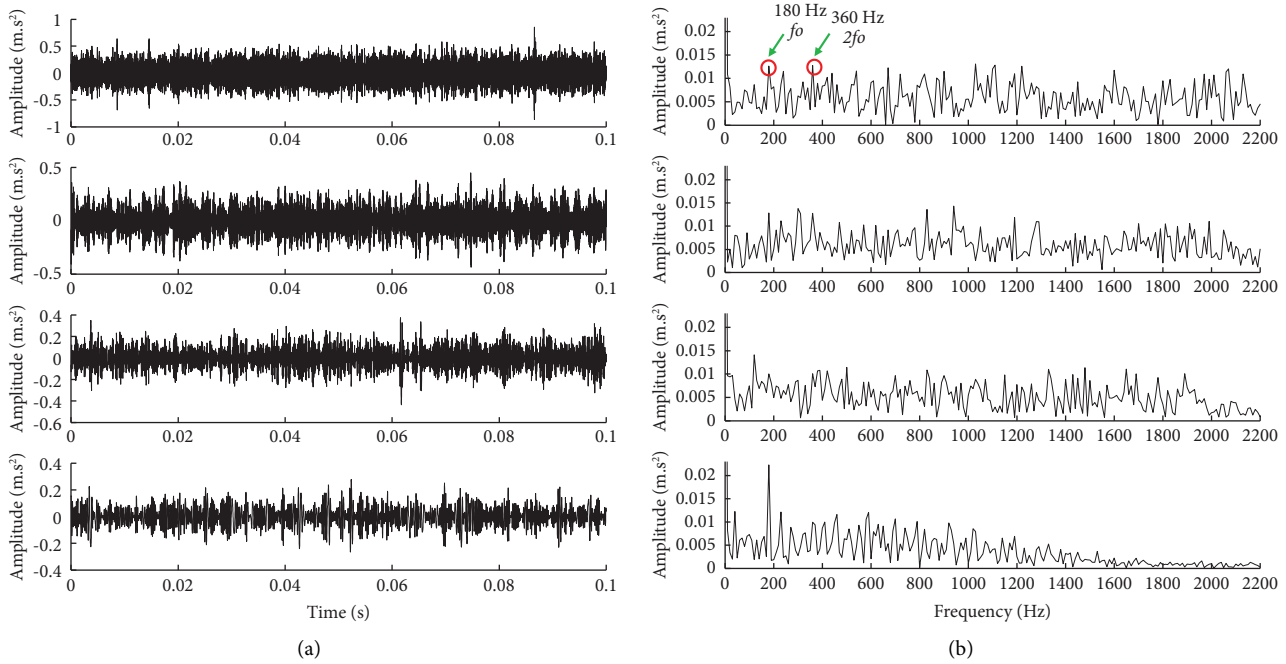

Figure 15: The result of decomposing the noise signal by EMD. (a) Time-domain waveform. (b) TKEO envelope spectrum.

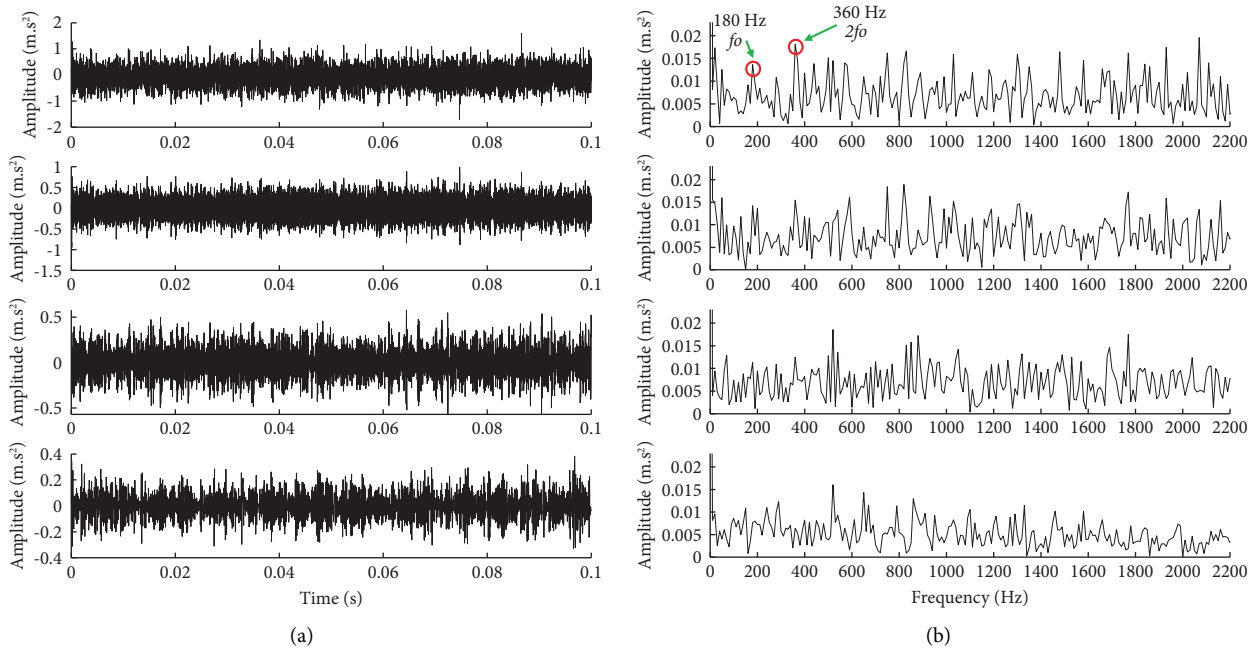

Figure 16: The result of decomposing the noise signal by EEMD. (a) Time-domain waveform. (b) TKEO envelope spectrum.

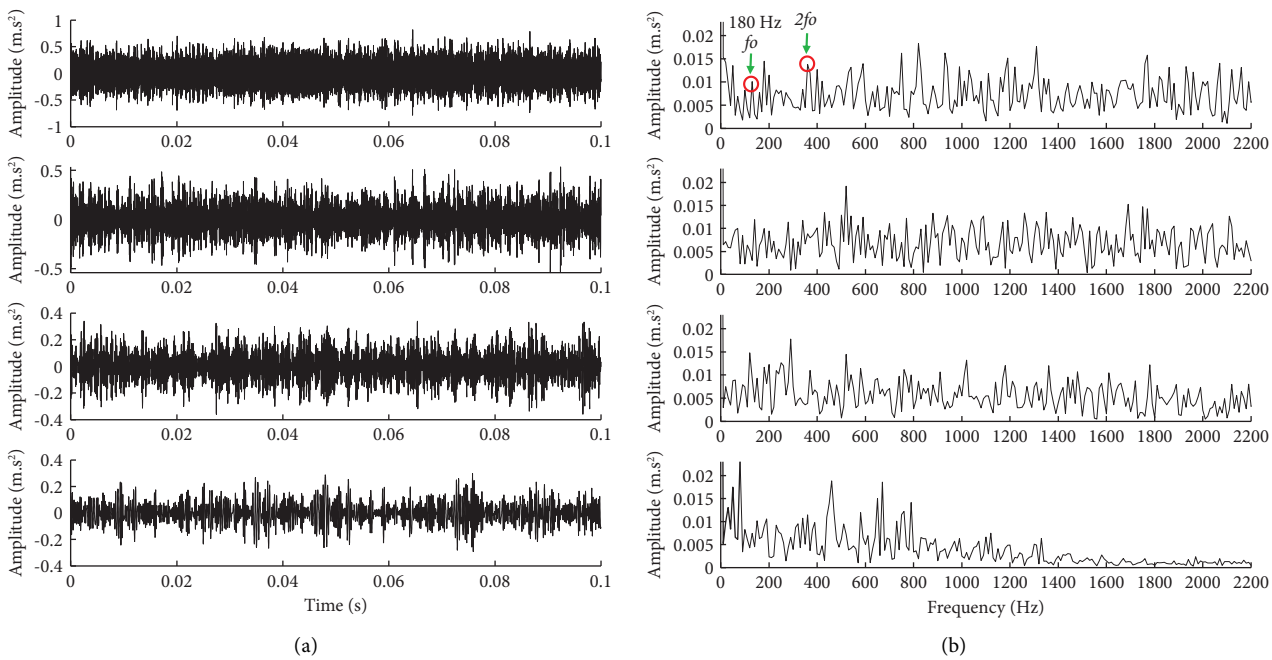

Figure 17: The result of decomposing the noise signal by CEEMDAN. (a) Time-domain waveform. (b) TKEO envelope spectrum.

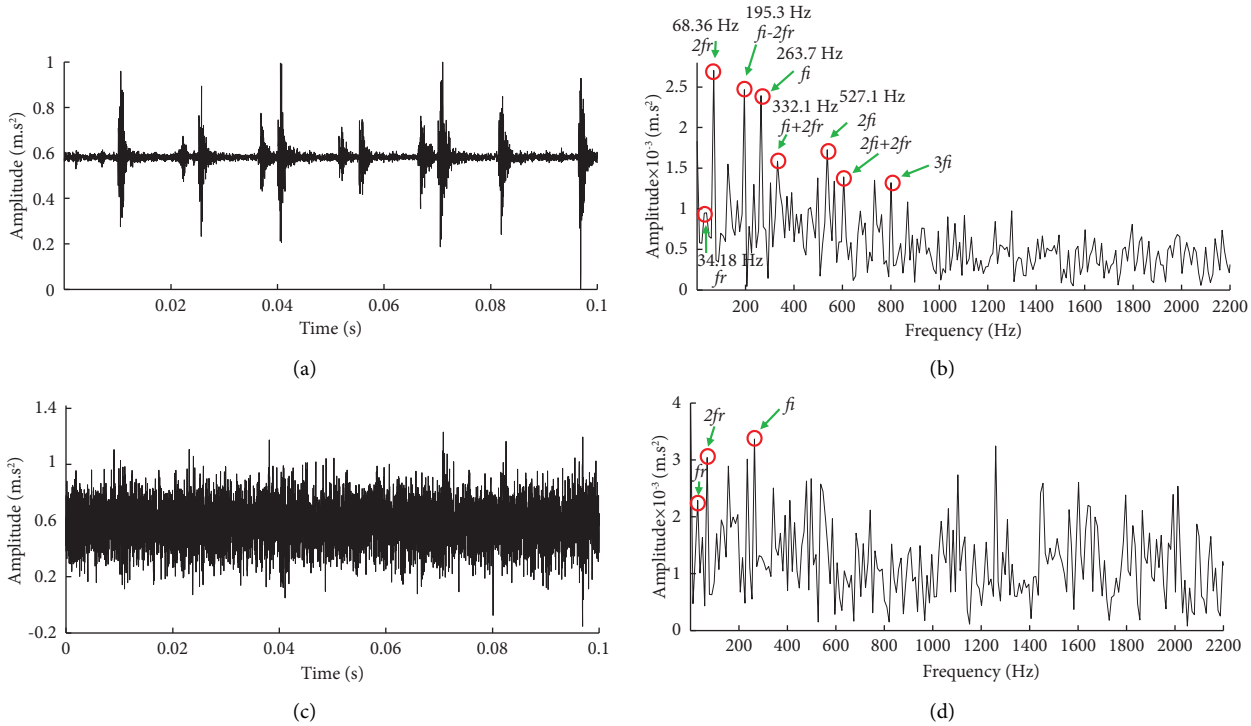

Figure 18: Time-domain waveform and TKEO envelope spectrum of inner ring defect. (a) Time-domain waveform of the origin signal. (b) TKEO envelope spectrum of the origin signal. (c) Time-domain waveform of the signal with added noise. (d) TKEO envelope spectrum of the noise signal.

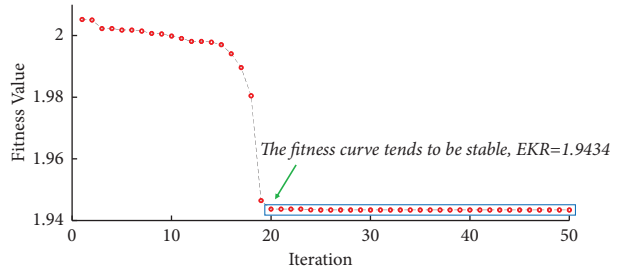

Figure 19: Fitness convergence curve.

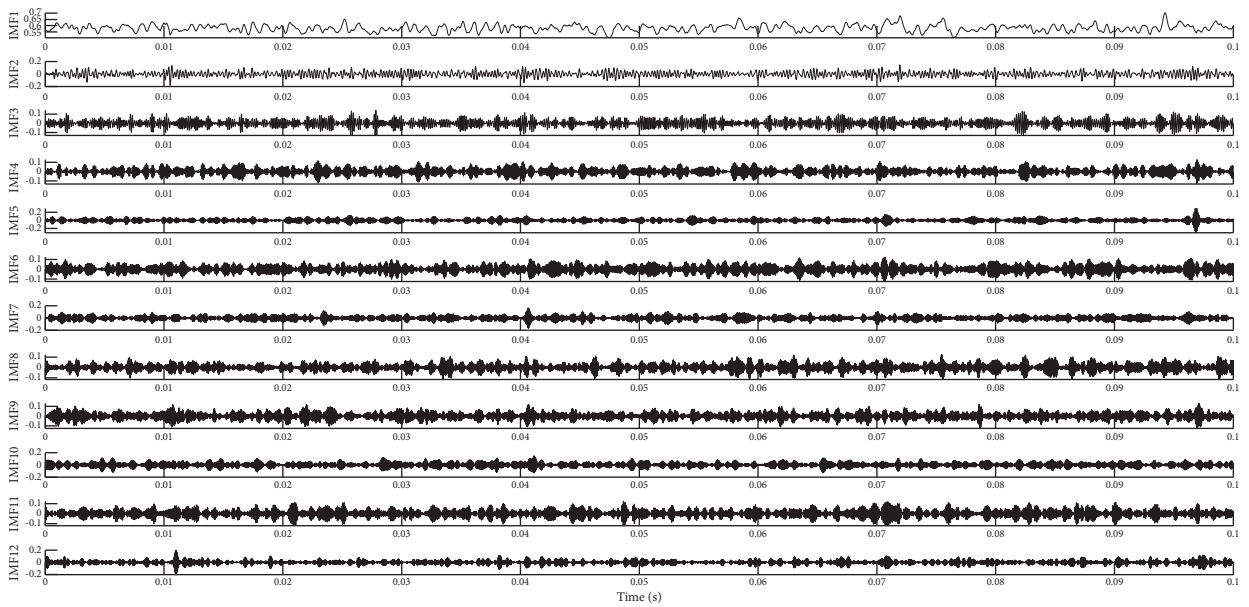

Figure 20: The result of decomposing the outer ring noise signal by VMD.

Table 6: The EKR value of each IMF.

IMF	EKR
IMF1	3.7158
IMF2	3.8513
IMF3	3.8517
IMF4	3.8260
IMF5	1.9434
IMF6	4.2623
IMF7	3.7740
IMF8	3.6369
IMF9	3.8396
IMF10	3.8728
IMF11	3.8302
IMF12	2.8748

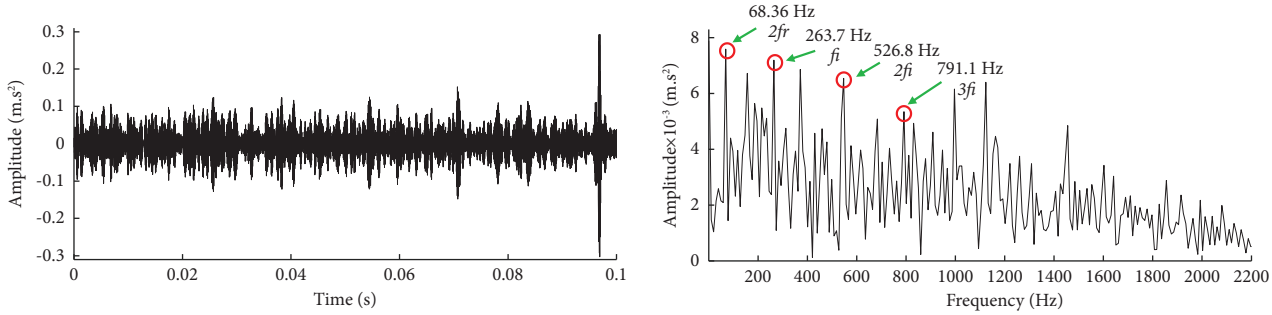

Figure 21: IMF5 reconstructed signal. (a) Time-domain waveform. (b) TKEO envelope spectrum.

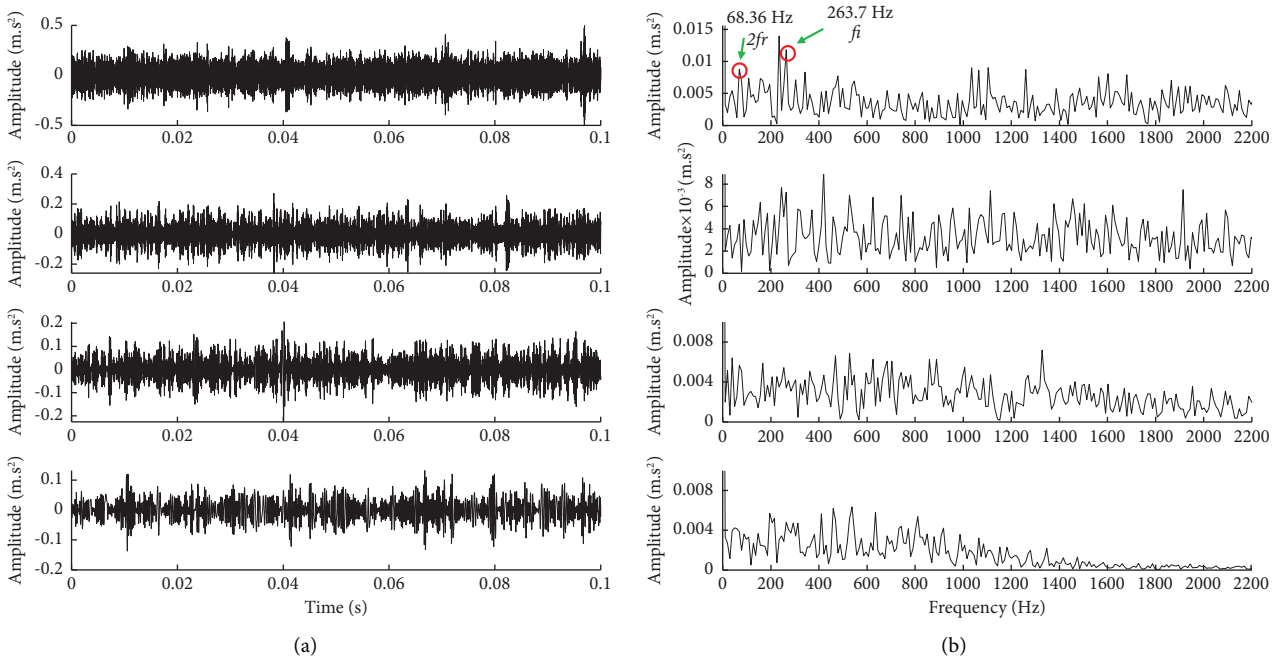

Figure 22: The result of decomposing the noise signal by EMD. (a) Time-domain waveform. (b) TKEO envelope spectrum.

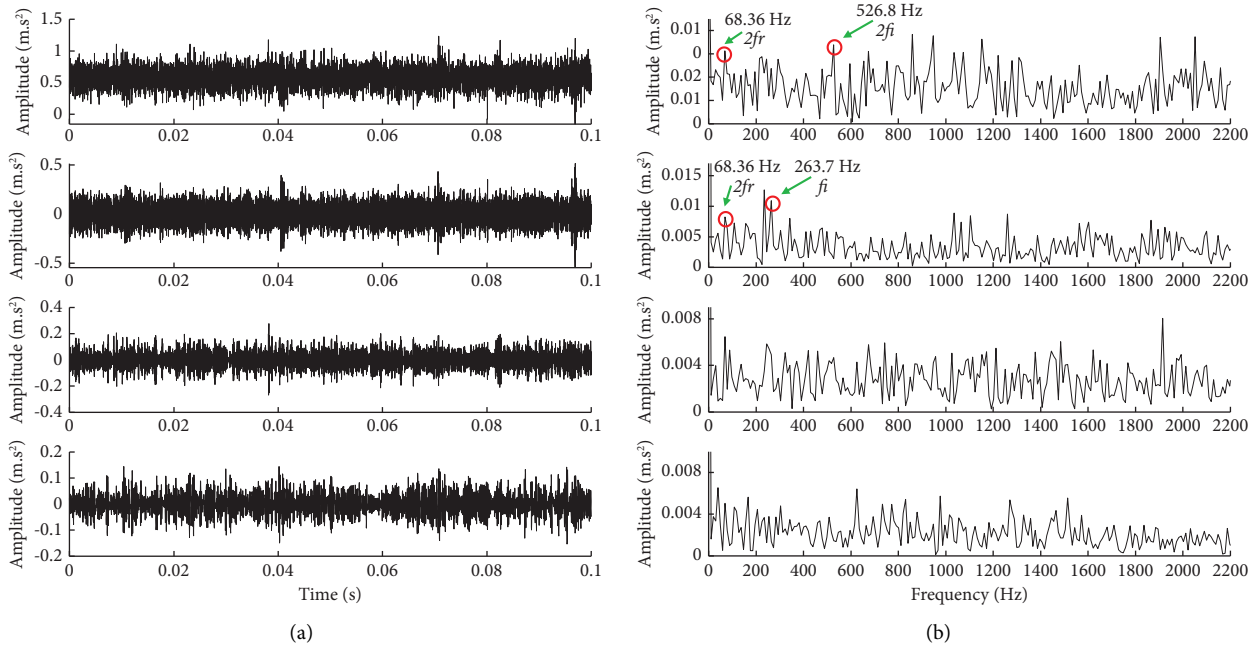

Figure 23: The result of decomposing the noise signal by EEMD. (a) Time-domain waveform. (b) TKEO envelope spectrum.

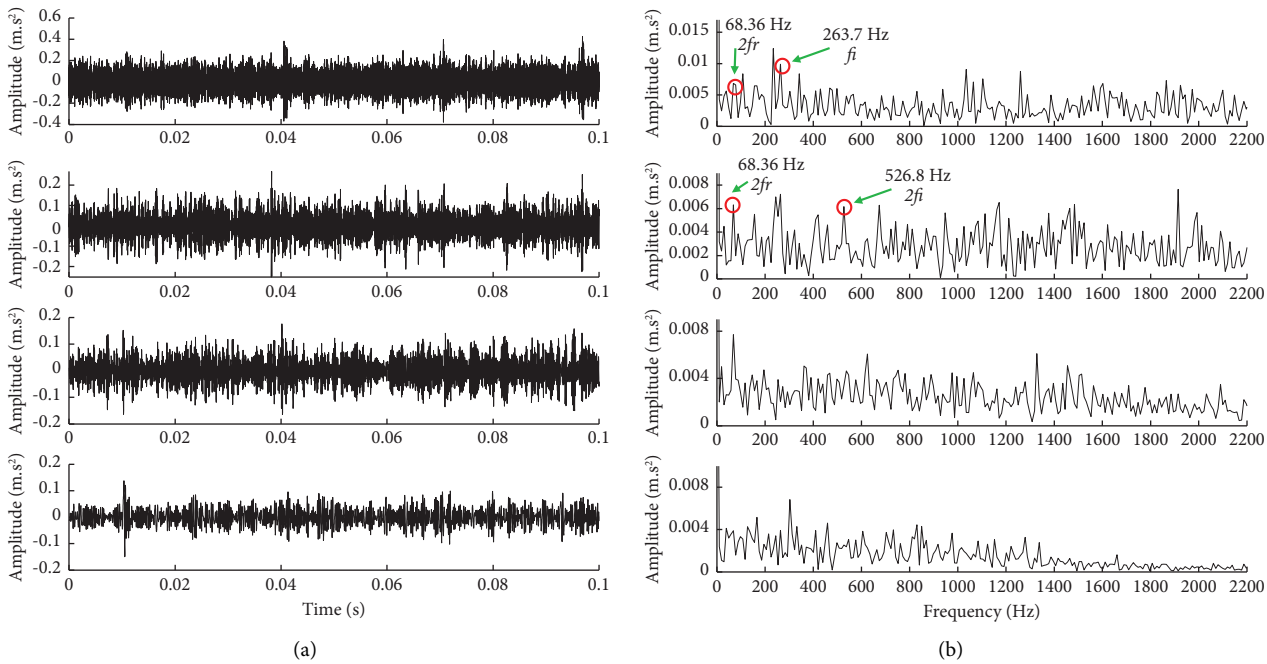

Figure 24: The result of decomposing the noise signal by CEEMDAN. (a) Time-domain waveform. (b) TKEO envelope spectrum.

CEEMDAN. As shown in Figure 24, the results of CEEMDAN are similar to those of EEMD. On the contrary, CEEMDAN performs better in terms of noise resistance.

Thus, the analysis of the inner ring fault signal further verifies the feasibility of the proposed method. At the same time, the comparison with the other three methods further confirms the superiority of this method.

6. Conclusions

This paper proposes a fault feature extraction method based on SOA-VMD to address the problem of weak bearing fault features and difficulty in selecting VMD parameters under noise interference. The feasibility of the method is verified by the simulation signals and experimental signals of rolling bearings, and it is compared with EMD, EEMD, and CEEMDAN methods. The results show that the proposed method has advantages in vibration analysis and fault feature extraction. The main conclusions are as follows:

(1) The EKR index is introduced as the fitness function of SOA, and the SOA is used to address the difficult problem of VMD parameter selection.

(2) Compared with EMD, EEMD, and CEEMDAN methods, the proposed method has more advantages in bearing fault feature extraction.

Data Availability

The data that support the findings of this study are available from the corresponding author upon reasonable request.

Conflicts of Interest

The authors declare that they have no conflicts of interest.

Acknowledgments

This work was supported by the Zhejiang Provincial Science and Technology Project under Grant no. KZS2101030 and the National Natural Science Foundation of China under Grant no. KZ1410067.

References

[1] T. Lin, G. Chen, W. Ouyang, Q. Zhang, H. Wang, and L. Chen, "Hyper-spherical distance discrimination: a novel data description method for aero-engine rolling bearing fault detection," *Mechanical Systems and Signal Processing*, vol. 109, pp. 330–351, 2018.

[2] C. Grover and N. Turk, "Rolling element bearing fault diagnosis using empirical mode decomposition and hjorth parameters," *Procedia Computer Science*, vol. 167, pp. 1484–1494, 2020.

[3] M. Han, Y. Wu, Y. Wang, and W. Liu, "Roller bearing fault diagnosis based on LMD and multi-scale symbolic dynamic information entropy," *Journal of Mechanical Science and Technology*, vol. 35, no. 5, pp. 1993–2005, 2021.

[4] F. Hemmati, M. Alqaradawi, and M. S. Gadala, "Rolling element bearing fault diagnostics using acoustic emission technique and advanced signal processing," *Proceedings of the Institution of Mechanical Engineers-Part J: Journal of Engineering Tribology*, vol. 230, no. 1, pp. 64–77, 2016.

[5] D. Liu, J. Tao, A. Luo, and Q. Wang, "An optimized kurtogram method for early fault detection of rolling element bearings using acoustic emission," in *Proceedings of the 2018 International Conference on Information Systems and Computer Aided Education (ICISCAE)*, pp. 365–370, Changchun, China, July 2018.

[6] N. E. Huang, Z. Shen, S. R. Long et al., "The empirical mode decomposition and the Hilbert spectrum for nonlinear and non-stationary time series analysis," *Proceedings of the Royal Society of London. Series A: Mathematical, Physical and Engineering Sciences*, vol. 454, no. 1971, pp. 903–995, 1998.

[7] R. Tabatabaei, A. Aasi, S. M. Jafari, and E. Ciulli, "Experimental investigation of the diagnosis of angular contact ball bearings using acoustic emission method and empirical mode decomposition," *Advances in Tribology*, vol. 2020, pp. 1–14, 2020.

[8] W. Chen and Y. Xiao, "An improved ABC algorithm and its application in bearing fault diagnosis with EEMD," *Algorithms*, vol. 12, no. 4, p. 72, 2019.

[9] Z. Wu and N. E. Huang, "Ensemble empirical mode decomposition: a noise-assisted data analysis method," *Advances in Adaptive Data Analysis*, vol. 01, no. 01, pp. 1–41, 2009.

[10] X. Zhang, Y. Liang, J. Zhou, and Y. zang, "A novel bearing fault diagnosis model integrated permutation entropy, ensemble empirical mode decomposition and optimized SVM," *Measurement*, vol. 69, pp. 164–179, 2015.

[11] X. Qin, Q. Li, X. Dong, and S. Lv, "The Fault diagnosis of rolling bearing based on ensemble empirical mode decomposition and random forest," *Shock and Vibration*, vol. 2017, pp. 2623081–9, 2017.

[12] D.-H. Lee, J.-H. Ahn, and B.-H. Koh, "Fault detection of bearing systems through EEMD and optimization algorithm," *Sensors*, vol. 17, no. 11, p. 2477, 2017.

[13] N. Lu, T. X. Zhou, J. F. Wei, W. L. Yuan, R. Q. Li, and M. L. Li, "Application of a whale optimized variational mode decomposition method based on envelope sample entropy in the fault diagnosis of rotating machinery," *Measurement Science and Technology*, vol. 33, no. 1, 2022.

[14] J. Zhang, R. Yan, R. X. Gao, and Z. Feng, "Performance enhancement of ensemble empirical mode decomposition," *Mechanical Systems and Signal Processing*, vol. 24, no. 7, pp. 2104–2123, 2010.

[15] J. Zheng, J. Cheng, and Y. Yang, "Partly ensemble empirical mode decomposition: an improved noise-assisted method for eliminating mode mixing," *Signal Processing*, vol. 96, pp. 362–374, 2014.

[16] K. Dragomiretskiy and D. Zosso, "Variational mode decomposition," *IEEE Transactions on Signal Processing*, vol. 62, no. 3, pp. 531–544, 2014.

[17] H. Wang, F. Wu, and L. Zhang, "Application of variational mode decomposition optimized with improved whale optimization algorithm in bearing failure diagnosis," *Alexandria Engineering Journal*, vol. 60, no. 5, pp. 4689–4699, 2021.

[18] S. Mohanty, K. K. Gupta, and K. S. Raju, "Comparative study between VMD and EMD in bearing fault diagnosis," in *Proceedings of the 2014 9th International Conference on Industrial and Information Systems (ICIIS)*, pp. 1–6, Gwalior, India, December 2014.

[19] M. Zhang, Z. Jiang, and K. Feng, "Research on variational mode decomposition in rolling bearings fault diagnosis of the multistage centrifugal pump," *Mechanical Systems and Signal Processing*, vol. 93, pp. 460–493, 2017.

[20] S. Zhang, Y. Wang, S. He, and Z. Jiang, "Bearing fault diagnosis based on variational mode decomposition and total variation denoising," *Measurement Science and Technology*, vol. 27, no. 7, 2016.

[21] S. Tan, A. Wang, H. Shi, and L. Guo, "Rolling bearing incipient fault detection via optimized VMD using mode mutual information," *International Journal of Control, Automation and Systems*, vol. 20, no. 4, pp. 1305–1315, 2022.

[22] J. Lian, Z. Liu, H. Wang, and X. Dong, "Adaptive variational mode decomposition method for signal processing based on mode characteristic," *Mechanical Systems and Signal Processing*, vol. 107, pp. 53–77, 2018.

[23] R. Gu, J. Chen, R. Hong, H. Wang, and W. Wu, "Incipient fault diagnosis of rolling bearings based on adaptive variational mode decomposition and Teager energy operator," *Measurement*, vol. 149, 2020.

[24] X. Zhang, Q. Miao, H. Zhang, and L. Wang, "A parameter-adaptive VMD method based on grasshopper optimization algorithm to analyze vibration signals from rotating machinery," *Mechanical Systems and Signal Processing*, vol. 108, pp. 58–72, 2018.

[25] C. Liu, L. Zhu, and C. Ni, "Chatter detection in milling process based on VMD and energy entropy," *Mechanical Systems and Signal Processing*, vol. 105, pp. 169–182, 2018.

[26] Y. Wang, P. Chen, Y. Zhao, and Y. Sun, "A denoising method for mining cable PD signal based on genetic algorithm optimization of VMD and wavelet threshold," *Sensors*, vol. 22, no. 23, p. 9386, 2022.

[27] J. Yang, C. Zhou, and X. Li, "Research on fault feature extraction method based on parameter optimized variational mode decomposition and robust independent component analysis," *Coatings*, vol. 12, no. 3, p. 419, 2022.

[28] C. Yi, Y. Lv, and Z. Dang, "a fault diagnosis scheme for rolling bearing based on particle swarm optimization in variational mode decomposition," *Shock and Vibration*, vol. 2016, pp. 1–10, 2016.

[29] H. Li, T. Liu, X. Wu, and Q. Chen, "An optimized VMD method and its applications in bearing fault diagnosis," *Measurement*, vol. 166, 2020.

[30] R. Shi, B. Wang, Z. Wang, J. Liu, X. Feng, and L. Dong, "Research on fault diagnosis of rolling bearings based on variational mode decomposition improved by the niche genetic algorithm," *Entropy*, vol. 24, no. 6, p. 825, 2022.

[31] T. Liang, H. Lu, and H. Sun, "Application of parameter optimized variational mode decomposition method in fault feature extraction of rolling bearing," *Entropy*, vol. 23, no. 5, p. 520, 2021.

[32] F. A. Hashim and A. G. Hussien, "Snake Optimizer: a novel meta-heuristic optimization algorithm," *Knowledge-Based Systems*, vol. 242, 2022.

[33] J. F. Kaiser, "On a simple algorithm to calculate the "energy" of a signal," *International Conference on Acoustics, Speech, and Signal Processing*, vol. 1, pp. 381–384, 1990.

[34] H. Wang, X. Jiang, W. Guo, J. Shi, and Z. Zhu, "An enhanced VMD with the guidance of envelope negentropy spectrum for bearing fault diagnosis," *Complexity*, vol. 2020, pp. 1–23, 2020.

[35] X. Jiang, J. Shi, W. Huang, and Z. Zhu, "Non-dominated solution set based on time–frequency infograms for local damage detection of rotating machines," *ISA Transactions*, vol. 92, pp. 213–227, 2019.

[36] X. Song, H. Wang, and P. Chen, "Weighted kurtosis-based VMD and improved frequency-weighted energy operator low-speed bearing-fault diagnosis," *Measurement Science and Technology*, vol. 32, no. 3, 2020.

[37] X. Zhang, Z. Luan, and X. Liu, "Fault diagnosis of rolling bearing based on kurtosis criterion VMD and modulo square threshold," *Journal of Engineering*, vol. 2019, no. 23, pp. 8685–8690, 2019.

[38] R. B. Randall, J. Antoni, and S. Chobsaard, "The relationship between spectral correlation and envelope analysis in the diagnostics of bearing faults and other cyclostationary machine signals," *Mechanical Systems and Signal Processing*, vol. 15, no. 5, pp. 945–962, 2001.

[39] J. Cheng, Y. Yang, X. Li, and J. Cheng, "Adaptive periodic mode decomposition and its application in rolling bearing fault diagnosis," *Mechanical Systems and Signal Processing*, vol. 161, 2021.

[40] N. Lu, M. Li, G. Zhang, R. Li, T. Zhou, and C. Su, "Fault feature extraction method for rotating machinery based on a CEEMDAN-LPP algorithm and synthetic maximum index," *Measurement*, vol. 189, 2022.

[41] A. Kumar, Y. Zhou, C. P. Gandhi, R. Kumar, and J. Xiang, "Bearing defect size assessment using wavelet transform based Deep Convolutional Neural Network (DCNN)," *Alexandria Engineering Journal*, vol. 59, no. 2, pp. 999–1012, 2020.

[42] A. Kumar and R. Kumar, "Enhancing weak defect features using undecimated and adaptive wavelet transform for estimation of roller defect size in a bearing," *Tribology Transactions*, vol. 60, no. 5, pp. 794–806, 2016.